



Mechanism of mine water inrush from overlying porous aquifer in Quaternary: a case study in Xinhe Coal Mine of Shandong Province, China

Huiyong Yin¹ · Han Zhao¹ · Daolei Xie¹ · Shizhen Sang¹ · Yongli Shi¹ · Maohu Tian²

Received: 26 June 2018 / Accepted: 1 February 2019 / Published online: 23 February 2019

© Saudi Society for Geosciences 2019

Abstract

Mine water inrush from coal seam roof is one of the serious disasters that threaten safe production of coal mines. Identification of water inrush source and water inrush pathway is a key task for preventing and controlling such mine water hazards. A water inrush accident at approximately 1316 m³/h occurred at no. 3301 working face of Xinhe Coal Mine in Shandong Province, China. Multiple lines of evidence including characteristics of mine water inflow rate, dynamic monitoring data of water levels in different aquifers, geochemical fingerprinting, and drill hole core examination suggest that the water inrush source originated from the overlying Lower Quaternary porous aquifer with calcite cementation. Structural analysis and numerical simulation with FLAC3D indicate that a low-angle fault, DF₄₉, and mining-induced fractures provided the pathway for the water inrush. Mining activities made the fault hydraulically conductive and connected to the Quaternary aquifer. The numerical simulation demonstrated that the water-conducting fracture zone in the coal seam roof extended to the fault. Groundwater gushed into the mining area from the Quaternary aquifer via the combined pathway of the activated fault and mining-induced fractures. Presence of the fault in the overlying formations played a critical role in occurrence of the water inrush. Results from this case study can be of reference to all coal mines with faults or other geological discontinuities present in the overlying formation. These discontinuities may significantly extend the height of the mining-induced water-conducting fracture zone in the roof and thus increase water inrush risks.

Keywords Fault activation · Numeric simulation · Water inrush · Water inrush source · Water inrush pathway

Editorial handling: Broder J. Merkel

Electronic supplementary material The online version of this article (<https://doi.org/10.1007/s12517-019-4325-0>) contains supplementary material, which is available to authorized users.

✉ Huiyong Yin
huiyongy@sdust.edu.cn

✉ Daolei Xie
skd994469@sdust.edu.cn

¹ Shandong Provincial Key Laboratory of Depositional Mineralization & Sedimentary Minerals, College of Earth Science & Engineering, Shandong University of Science and Technology, Qingdao 266590, China

² Shandong Xinhe Mining Co., Ltd., Jining 272400, China

Introduction

China's coal production is ranked first in the world, but it is also one of the countries with the worst safety records (Guo 2016). As one of the safety concerns, mine water inrush affects the safety of mine production and people's property seriously (Wei et al. 2015; Sun et al. 2016; Wei et al. 2017; Yang et al. 2017; Wu et al. 2017a; Yin et al. 2018a). The water inrush may occur from coal seam floor or roof. Due to various geological and hydrogeological conditions and complex tectonics structures of the coalfields in China, causes and mechanisms of mine water inrush vary significantly (Zhang 2005; Sun et al. 2015; Qi et al. 2017; Zhang et al. 2018b). Especially with the large-scale exploitation of coal resources in recent years, the water hazards prevention and control has been highly demanded (Yin et al. 2018b; Xu et al. 2018). Among the many tasks and challenges, the prevention and control of water hazards is a major scientific research topic during China's coal mine safe production and scientific

exploration (Miao et al. 2010; Jin et al. 2013; LaMoreaux et al. 2014; Wu et al. 2017a; Zhou et al. 2017).

China's coal mining has been intensive in recent years. More and more coal mines are forced to tap deeper resources or shallower resources in remote areas (Zhang et al. 2018a; Xu et al. 2018). However, the difficulty of prevention and control of mine water hazards increases because the geological and hydrogeological conditions are more complex in deeper areas (Wu et al. 2013; Zhao et al. 2012). Mine water accidents have occurred during exploitation of shallow coal resources when the underground workings are connected with the overlying aquifers.

In response to this challenge, a series of research have been conducted including theoretical analysis, numerical simulation, and field measurement (Tan et al. 2012; Li et al. 2013; Jiang et al. 2016; Wu et al. 2008; Bukowski 2011; Rapantova et al. 2012; Surinaidu et al. 2013; Krzysztof et al. 2016; Yin et al. 2016; Guo et al. 2017). Recently, mining using remote sensing and GIS leads to solving problems related to water sources based on element characteristics (Cetin 2016; Kaya et al. 2018; Cetin et al. 2018). Zhang et al. (2005) applied the GIS-based composite analysis method to forecast roof water damage, which provides a new method for roof water hazard prediction. Huang and Chen (2011) established the Fisher identification and mixing models of mine water inrush sources based on multivariate statistical analysis, and verified them separately. Based on Fisher discriminant analysis theory (FDA) and gray correlation analysis theory (GCA), and groundwater chemical data at main water inrush aquifers, Huang et al. (2017a, b) established and then verified the FDA-GCA recognition model of water inrush source. Xu et al. (2012) used field monitoring and numerical simulation to study the mining failure and the formation and evolution process of the water inrush pathway in coal seam with highly confined water. Li et al. (2009) applied the simulation analysis to study the formation process of the water inrush pathway in coal seam floor with faults. Zhang et al. (2017a) applied fluid-solid coupling mechanics and solid materials research to simulate the entire process of crack formation, concealed fault propagation, and evolution of a water inrush channel with high-pressure water directly beneath the mine floor. By using numerical simulation (RFPA2D) methods, Bu (2009) established the rock seepage-damage coupling model, simulated the characteristics of floor fault activation and seepage distribution with normal fault and reverse faults, and analyzed the influence of fault inclination, fault drop, and water pressure on the risk of water inrush from the floor. Xu et al. (2015) established a simplified model of reverse faults, which revealed the basic action of the fault parameters during mining with FLAC3D software.

Extensive studies have been conducted on the confined aquifers underlying the coal seam floor such as the Ordovician limestone aquifer and activation of normal faults with high dip angles such as the movement of hanging wall of normal faults. Furthermore, much research has been conducted into how coal mine water hazards result from coal seam roof

because of mining-induced water conducting fracture zone in the coal seam roof. However, the movement and activation of low dip angle normal faults in the coal seam roof in response to mining have not been studied. These distinctive conditions deserve special considerations. When these discontinuities are present and become conductive during mining, they may become the conduit that connects the mining-induced water conducting zone to the overlying Quaternary porous aquifer, which significantly increases water inrush risks.

Although the previous researches have raised awareness of underground water inrush, it is still impossible to accurately predict the position and time of accidents owing to the complexity of hydrogeological conditions. Therefore, mine water inrush mechanism is still the key issue that needs to be studied and improved (Sui et al. 2011; Qi et al. 2017). A mine water inrush accident of approximately 1316 m³/h occurred during mining at the no. 3301 working face in Xinhe Coal Mine (CM). The source of water inrush and the water inrush pathway, the process of fault activation in low-angle fault footwall mining, and the roof water seepage transformation mechanism were studied in this article. The objective of this research was to analyze the causes of water inrush, and to study the formation process of water inrush source and water inrush pathway. FLAC3D modeling was used to study the activation of the footwall in the low-angle normal fault and the transformation of the roof water seepage, which reveals the mechanism of mine water hazard from the coal seam roof.

Characteristics of the study area

Background of Xinhe CM

Xinhe CM is located at approximately 7.5 km east of Jiayang County, west of Jining City, Shandong province. On average, its north–south length is 5.5 km and its east–west width is 3.0 km. The site lies between 116° 26' 35" E and 116° 28' 53" E longitude and 35° 22' 16" N and 35° 25' 40" N latitude and covers an area of approximately 10 km² (Fig. 1). Its mining depth is from –180 to –1300 m. The mining activities have focused on coal bed no. 3 (CB3), which belongs to the Permian Shanxi Formation (F).

Geologic and hydrogeological setting

Xinhe CM is in a typical North China coalfield of Permo-Carboniferous age. The mined coal beds belong to the Taiyuan and Shanxi Fs, which overlie the middle Ordovician limestone. The coal-bearing deposits are attributed to the Benxi F, Taiyuan F, Shanxi F, and Shihezi F, which are overlaid by the Quaternary deposits, as shown in Fig. 2.

Xinhe CM is in the southwest boundary of Tangkou district in Jining coalfield, where faults were more developed in the minefield. A total of 144 faults were reported from geo-

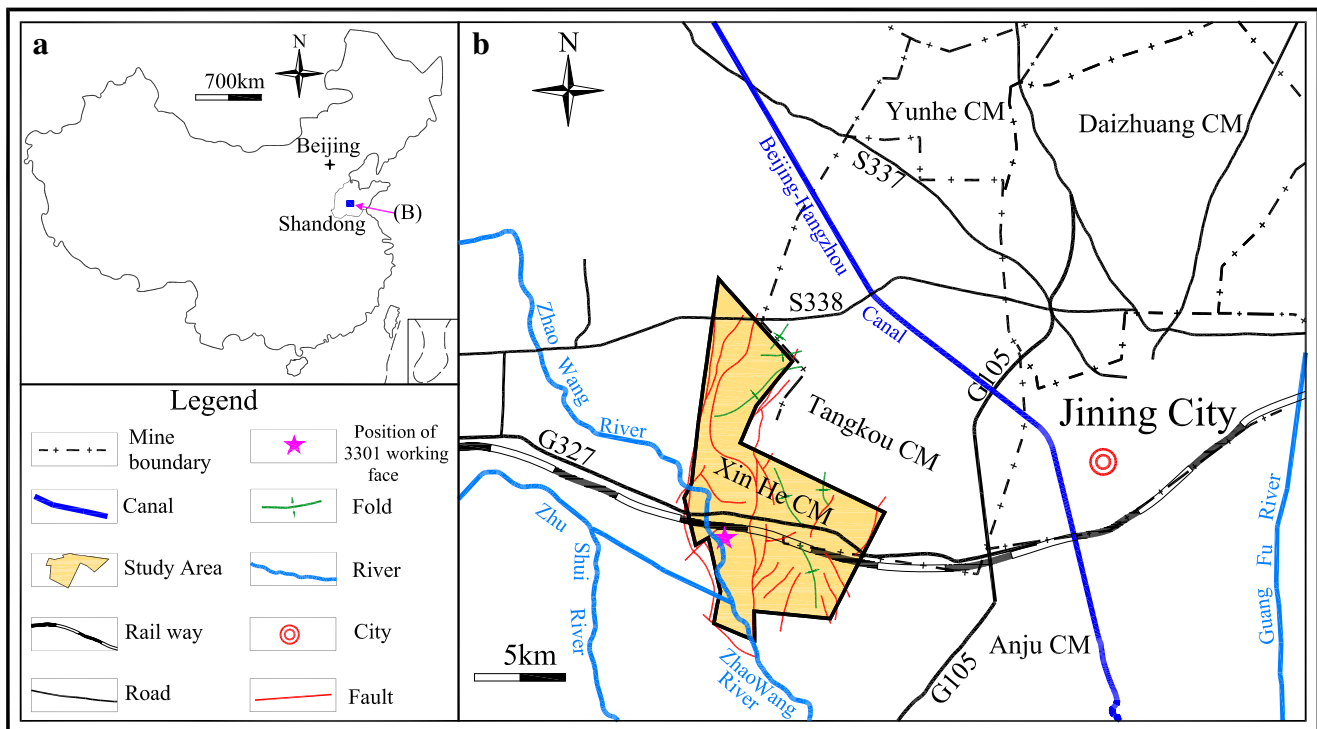


Fig. 1 Location map of the study area

exploration and interpretation of 3D seismic survey. Thirty-two faults were actually exposed in the mining process. According to the strike of the faults, they can be divided into three groups: near North–South, North–East, and North–West. Many faults have impacted the production and safety in Xinhe CM.

As shown in Fig. 2, the main aquifers from top to bottom are Quaternary sand and gravel aquifer, sandstone aquifers at the roof and floor of CB3, the 3rd limestone karst fissure aquifer, the 10th limestone karst fissure aquifer, and limestone karst fissure aquifer in the Ordovician formation. The sandstone aquifer at the CB3 roof is the impactive aquifer during the CB3 mining with the normal inflow rate at approximately $70 \text{ m}^3/\text{h}$. However, the maximum water inrush quantity at 3301 working face is up to $1316 \text{ m}^3/\text{h}$ and forced to stop mining in Xinhe CM (Figs. 3 and 4).

Based on the borehole data, the Quaternary formation is 240.3 m thick with 15.9 m conglomerate at the bottom. The core samples show cavities ranging from 10 to 40 mm in size and fracture length in 10 to 40 mm, as shown in Fig. 5.

The lower part of the Quaternary deposits is comprised of gray white calcium clay, calcareous clay and calcareous cemented layer, gray green clay, and clayey sand and gravel. The upper part consists of hard calcareous sand with weak consolidation. In boreholes on the southern and western edges of the site, the calcium content is high. The calcareous layer at the bottom was partially consolidated into calcareous tuberculosis or conglomerate due to the calcite cementation. During the deposition process, cobbles and cemented minerals were solidified and transformed into a cemented layer accompanied

by dissolution, cementation, adhesion, and consolidation. These layers are located outside the paleochannel.

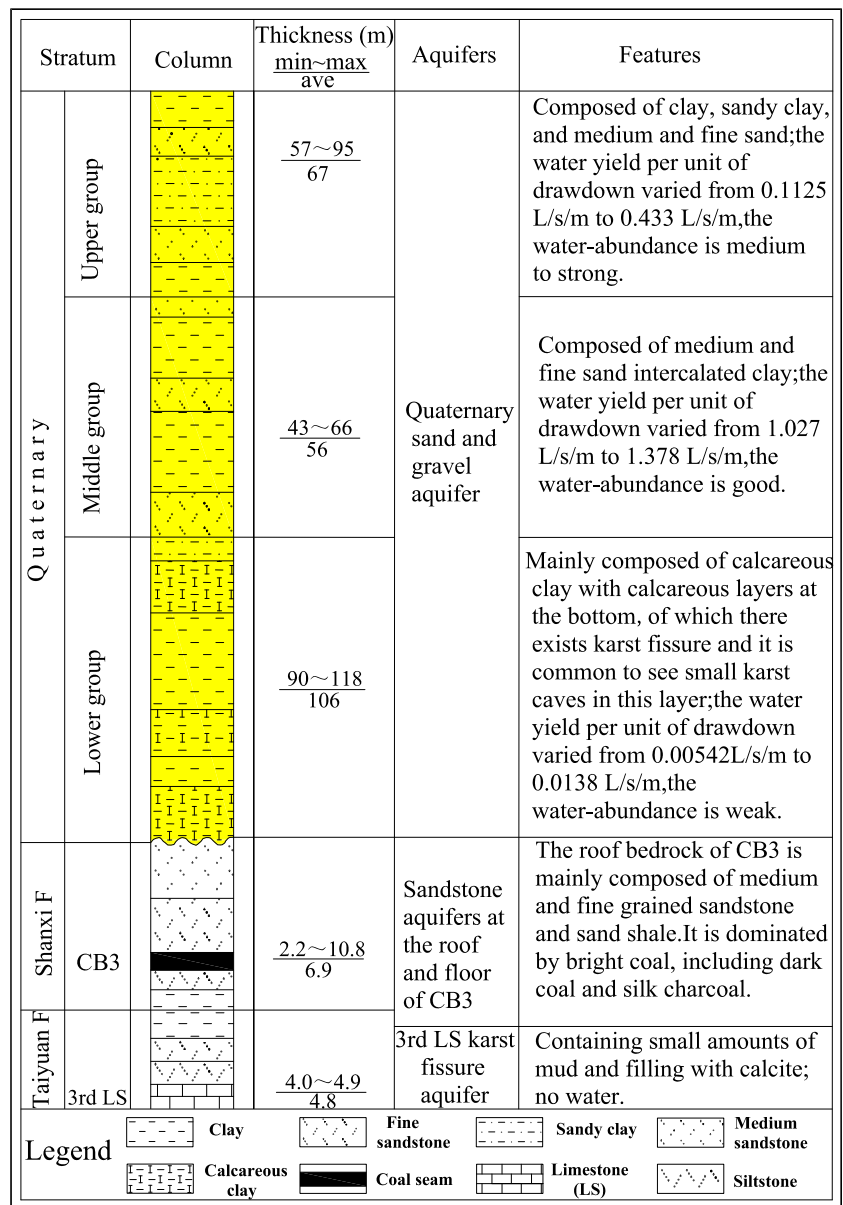
Karst features such as solution cavities were observed in the calcareous layer of the lower group in the Quaternary formation. The karst cavities result from long-term dissolution of the calcite cementation. The layer is characterized with yellow rust color, and the maximum thickness is 17.55 m. The diameter of the karst cavities exposed in exploration borehole no. JC3 ranges from 10 to 40 mm (Fig. 5). Calcite crystals of different sizes are present in the karst cavities. The karstification rate is estimated to be more than 30%. The cavernous porosity of the breccia layer is 15 to 20%. Approximately 36% of the exploration boreholes lost circulation in the bottom calcareous layer. All boreholes lost circulation in the bottom gravel layer, and the leakage is more than $15 \text{ m}^3/\text{h}$. Analysis of pumping test results in specific water yield of 4.427 L/s/m and permeability coefficient of 36.87 m/day . The permeability coefficient and porosity increase because of the karstification, which increase the groundwater storage and flow rate in the aquifer (Huang et al. 2017a, b; Chen et al. 2018).

Introduction to the 3301 working face and water inrush characteristics

Brief introduction to the 3301 working face

The 3301 working face is located at the middle of the Xinhe CM. The elevation of the CB3 floor ranges from -243 to -367 m, and with the average depth of 331 m. The average coal

Fig. 2 Hydrogeological histogram



seam angle of the working face is approximately 20°, and the average coal seam thickness is 6.9 m. The mining method is fully mechanized thick limit caving and short wall retreat. The geological structure of the working face is relatively simple where four faults were revealed with displacements ranging from 3 to 25 m. The faults are normal faults. The 3301 working face is the first mining face of the no. 330 mining area located in the DF₄₉ fault footwall, as shown in Fig. 3.

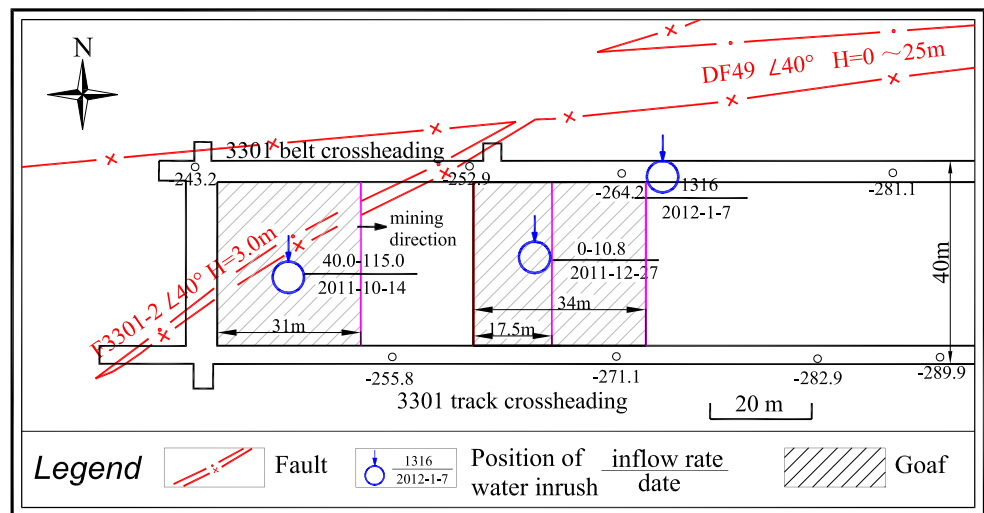
Description of the water inrush process

At 6:30 on October 14, 2011, there occurred the water inrush from CB3 roof after the first main roof pressure and crush the whole bracket for 3 h at the 3301 working face. The mine water flow rate increased rapidly from the initial 18 m³/h to

the maximum of 115 m³/h at 10 o'clock, and then gradually decreased. Water quality test results show that the water is from the sandstone aquifer at the CB3 roof. By October 25, the water flow rate declined to 40 m³/h.

The working face continued mining on December 23, 2011, and the roof pressure was basically stable. At 13:30 on December 27, 2011, the mine water discharged from the CB3 roof after the track along the chute out. The total discharge rate was 45.7 m³/h and remained stable from 16:00 December 27 to 18:00 December 28. The water discharge increased to 53 m³/h when the working face advanced 23 m on January 2, 2012. The amount of mine water varied from 60 to 121 m³/h from January 3 to 6. The water quality test result verified that the water was still from the sandstone aquifer at the CB3 roof. At 17:00 January 7, the fore-field coal wall

Fig. 3 3301 working face water inrush point schematic



suddenly collapsed 3 m from the belt crossheading along the roof and then the amount of mine water increased rapidly from to 1254 m³/h by 22:00 the same day. The maximum flow rate was 1316 m³/h at 12:00 pm January 8. After that, the water inflow rate dropped rapidly. The flow rate varied from 170 to 200 m³/h on January 17. On January 24, the water flow rate decreased to 150 m³/h.

Analysis of water inrush mechanism

The most critical factors in water inrush analysis are to identify the mine water inrush source and pathway in order to understand the groundwater inrush and save the mine for a long-term safe operation (Wu et al. 2017b; Xu et al. 2018).

Water inrush source

Five aquifers are recognized in the minefield, and they are shown in Fig. 6 and described below:

1. Quaternary sand and gravel aquifer: This aquifer consists of three groups. The upper group: total dissolved solid (TDS) is about 500 mg/L, and the water quality type is HCO₃⁻·SO₄²⁻·Ca²⁺·Na⁺. The middle group: the sand pore aquifer of this group has no hydraulic connection with the water aquifer of the lower group. The lower group: TDS is 676~700 mg/L, and water quality type is dominated by HCO₃⁻·SO₄²⁻·Ca²⁺·Mg²⁺·Na⁺.
2. Sandstone aquifers at the roof and floor of CB3: TDS is 400~741 mg/L, belonging to HCO₃⁻·Na⁺-type water.

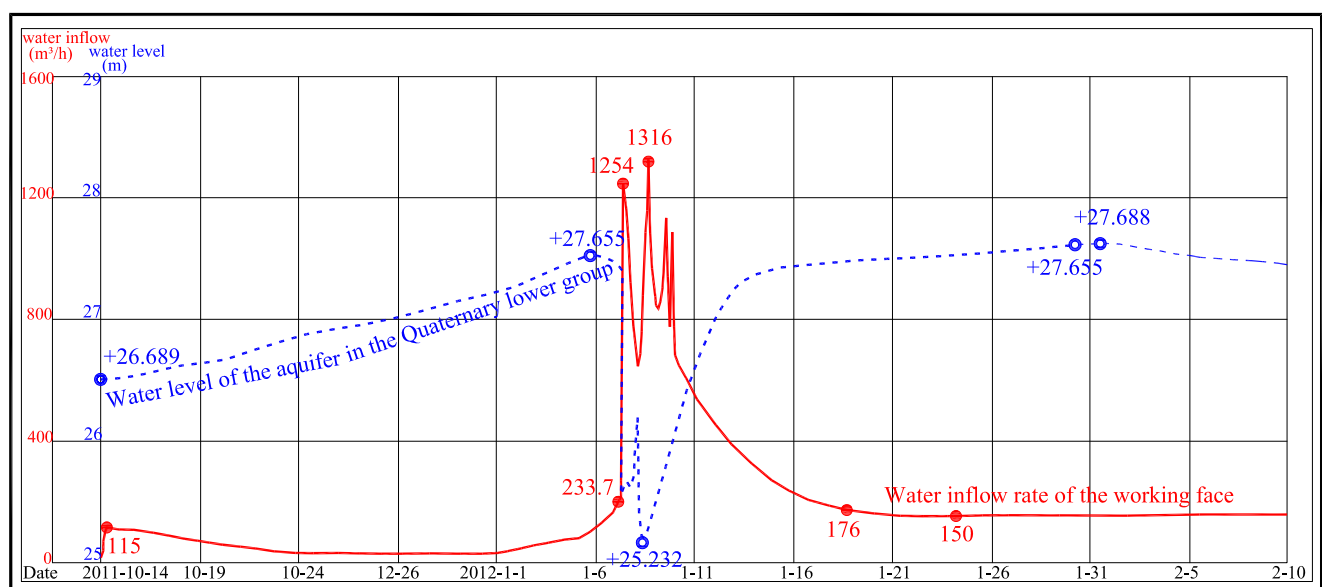
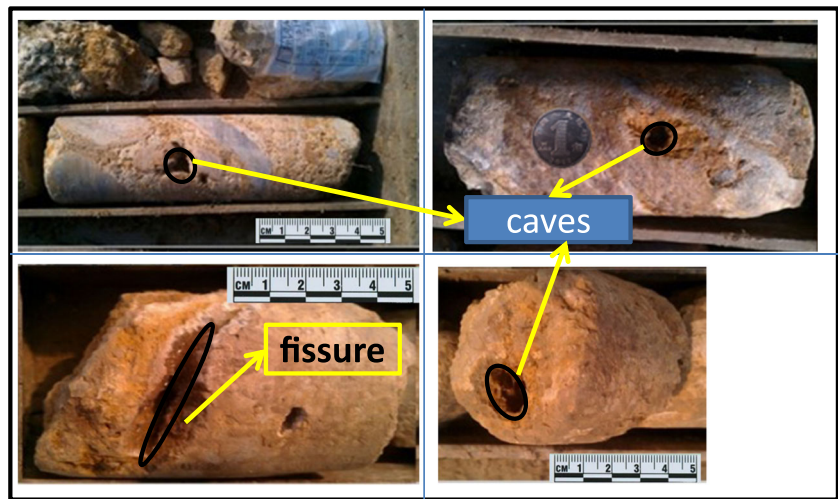


Fig. 4 3301 working face water volume and the aquifer water level curve

Fig. 5 Distribution of caves and fissures of aquifers in the Quaternary



- 3. Third limestone karst fissure aquifer: TDS is 667 mg/L, belonging to $\text{HCO}_3^- \cdot \text{Na}^+$ -type water.
- 4. Tenth limestone karst fissure aquifer: TDS is 3347 mg/L, and the water quality type is $\text{Cl}^- \cdot \text{SO}_4^{2-} \cdot \text{Ca}^{2+} \cdot \text{Na}^+ \cdot \text{Mg}^{2+}$.

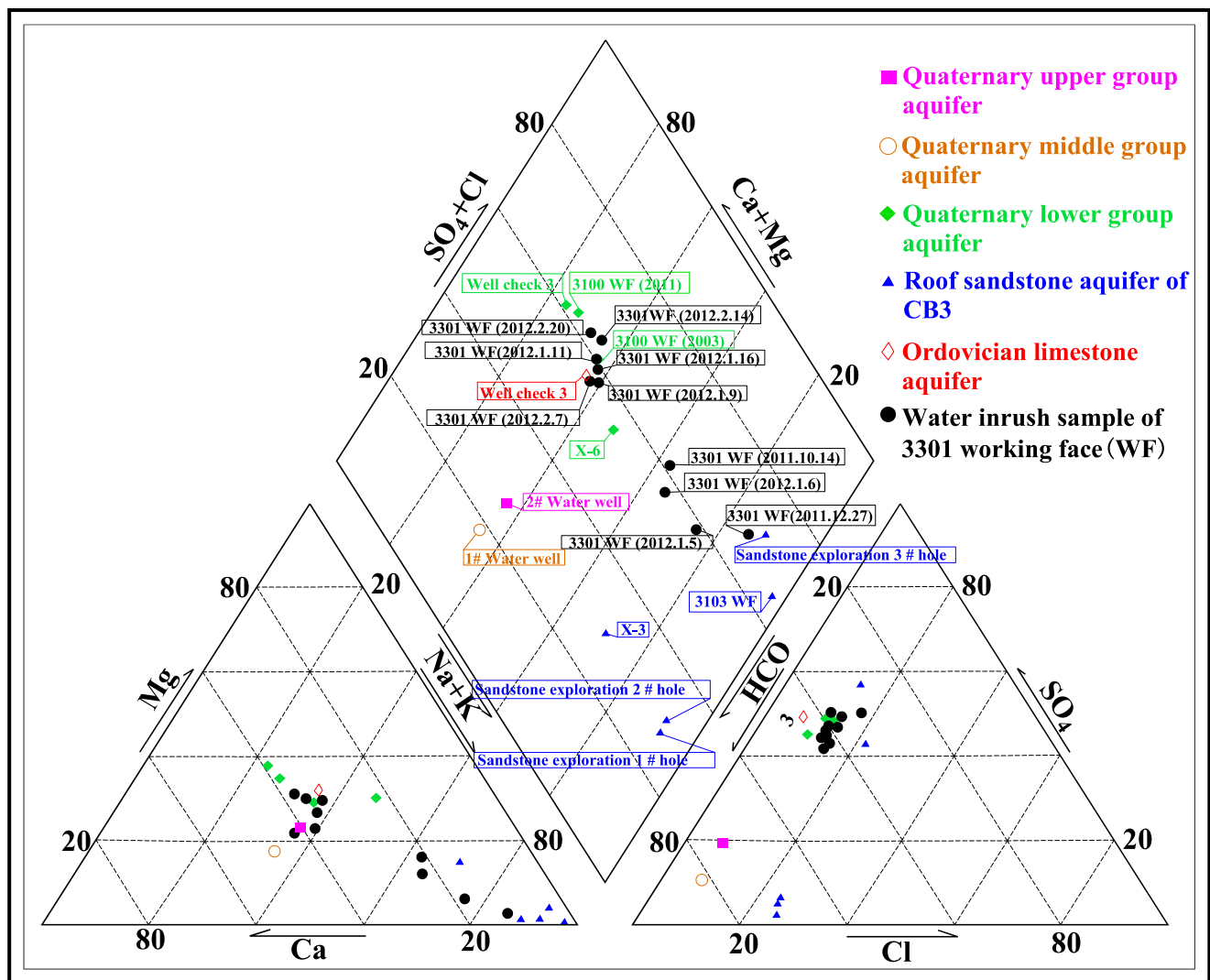


Fig. 6 Water chemistry Piper diagram

5. Limestone karst fissure aquifer in the Ordovician formation: TDS ranges from 1052 to 5366 mg/L, and the water quality type is $\text{SO}_4^{2-}\cdot\text{Cl}^-\cdot\text{Ca}^{2+}\cdot\text{Na}^+\cdot\text{Mg}^{2+}$.

After the water inrush, it was observed that there was no significant change in the water level of the surface subsidence area near the 3301 working face. The possibility of surface water recharge was excluded. The water level of seven farm water wells in the vicinity of the 3301 working face did not show noticeable decrease (please see electronic supplementary material, Fig. 9). The possibility of water recharge from the upper group aquifer in the Quaternary deposits was basically ruled out as well.

However, the water level of the lower group aquifer in the Quaternary deposits corresponded to the change of water inrush quantity, which indicates that the water inrush source is closely related to the calcareous layer and gravel layer at the lower group aquifer in the Quaternary deposits, as shown in Fig. 4.

In addition to the water level data, the water quality test data provided another piece of evidence to identify the source of mine water inrush (Wu et al. 2017b; Xu et al. 2018). The mine water quality data suggests that the mine water inrush source was the sandstone aquifer on the CB3 roof before January 6, 2012. On January 7, after the sudden increase in water volume in the working face, the water quality was similar to the lower group calcareous layer of the Quaternary formation. As shown in the water chemistry Piper diagram of Fig. 6, the Ca^{2+} concentration is relatively high, while the previous water sample data shows that the Ca^{2+} concentration is relatively low. All the test data indicate that the source of mine water inrush originated from the lower group calcareous layer of the Quaternary formation.

In summary, the large water flow rates in the water inrush were supported by and supplied from the calcareous aquifer at the lower group in the Quaternary formation. The aquifer is heterogeneous with strong groundwater abundance above the 3301 working face. There may be a strong karst fissure water passage or an ancient river bed water passage in the calcareous or gravel layer at the bottom of Quaternary formation.

Water inrush pathway

Water inrush source and pathways are indispensable factors to have the water inrush accident. Similar to identification of the water inrush source, it is difficult to detect exactly the mine water inrush pathways (Wang et al. 2017; Sun et al. 2017; Qiao et al. 2017). The common water inrush pathways include faults, mining-induced fractures, karst collapse columns, and poor sealing boreholes, but the majority of the water inrush pathways are faults (Zhang et al. 2016; Zhang et al. 2017b; Zhang et al. 2017c; Yu et al. 2017; Zhou et al. 2017). According to the site conditions, this paper considers two aspects in determining the pathway: water-conducting fracture zones and faults.

Water-conducting fracture zones

The average uniaxial compressive strength of the main roof of CB3 is 52.56 MPa. With reference to the latest version “Guideline for coal pillar retention and pressure coal mining in buildings, water bodies, railways and major roadways,” hereinafter referred to as “Guidelines” (State Coal Industry Bureau 2017), the CB3 roof is more reasonably hard. The empirical formula to calculate the height of the water-conducting fracture zone is

$$H_{Li} = \frac{100M}{1.2M + 2.0}$$

where H_{Li} is the maximum height of water-conducting fracture zones (m), and M is the mining thickness (m).

Applying the CB3 mining height of 5.0 m to the above formula results in the maximum height of the water-conducting fracture zone of 62 m.

All the aquifers in the area of 3301 working face overlying CB3 constitute the water recharge source. Since CB3 is approximately 80 to 100 m away from the bottom of the Quaternary formation in the upper part, the height of the water-conducting fracture cannot connect to the Quaternary aquifers under normal circumstances, namely, with the presence of impermeable layers. Therefore, the water-conducting fracture zone cannot be the water inrush pathway alone.

Faults

Fault DF₄₉ was previously exposed nine times in 3100, 3104, and 3301 working faces and –400-m level tunnel, and no water was encountered. Three roof holes were drilled through the excavation in the 3301 working face, and none of them encountered water. Fault DF₄₉ was directly exposed at two positions in the 3301 working face, and no water was observed. However, the water inrush occurred near the fault zone during the 3301 working face mining. The 3301 working face is located on the lower plate of fault DF₄₉. Mining activities caused the originally inactive DF₄₉ fault to activate, especially under the low dip fault, triggering the water inrush.

In the process of mining the low-angle fault footwall, the roof of the mined-out area subsided by gravity. Hindering the roof sinking is mainly the fault plane between the hanging wall and footwall cementation cohesion. Smaller angles indicate greater fault cohesion to withstand the gravity and the degree of fracture of the fault plane under certain conditions. And smaller angles are more susceptible to activation of the fault. In response to mining at the 3301 working face, the immediate overlying rock caved and fractures above the caving zone extended to the fault location, leading to fault stress state changes, The fault plane and the surrounding fissure expanded, and plastic damage occurred in the fault plane and the upper part of the contact with the

Quaternary area, resulting in greatly enhanced permeability in the fault and plastic damage zone. The permeable zone could be an important pathway for the conductive Quaternary base aquifer. On the other hand, the bottom of the Quaternary formation is strong aquifer overlying the fault. Under the condition of water–rock interaction, the seepage is concentrated on the fault plane. When the top seepage area and fault plane and fracture are hydraulically connected, the Quaternary water could flow in the work space along the fault and water-conducting fracture zones, causing the water inrush accident (Fig. 7).

Reasons of water inrush

In conclusion, the main causes of water inrush in 3301 working face are as follows: (1) there is a local water abundance area in the calcite cementation aquifer of the Lower Quaternary formation, which constitutes the source of the water inrush, and (2) coal mining caused activation of low dip fault DF₄₉ which constitutes the flow path of the water inrush.

Fault activation mechanism of low-angle normal fault in response to footwall mining

Fault is a geological structure that underwent a significant displacement along the rupture surface along the rock mass during the geological movement after the formation of the rock mass. The structure around the fault is called a fault fracture zone, and its cross section can be divided into two zones: tectonic rock zones and influence belt of faults (Lei et al. 2016; Zhou et al. 2017). The influence belt of faults is fractured zones affected by faults, distributed on both sides of the tectonic rock zones, and its width depends on the size of the fault and the mechanical properties of the two rocks and

other factors. Under influence of mining activities, the fault will be re-active or activated. After the fault activation, the stress and fracture of the fault zone change. The original water-free formation is replaced by water-conducting fracture zones, even with caving zone water guide passage being formed between the aqueous layer and the stope, causing water inrush accidents (Cheng et al. 2013; Zhang et al. 2017a).

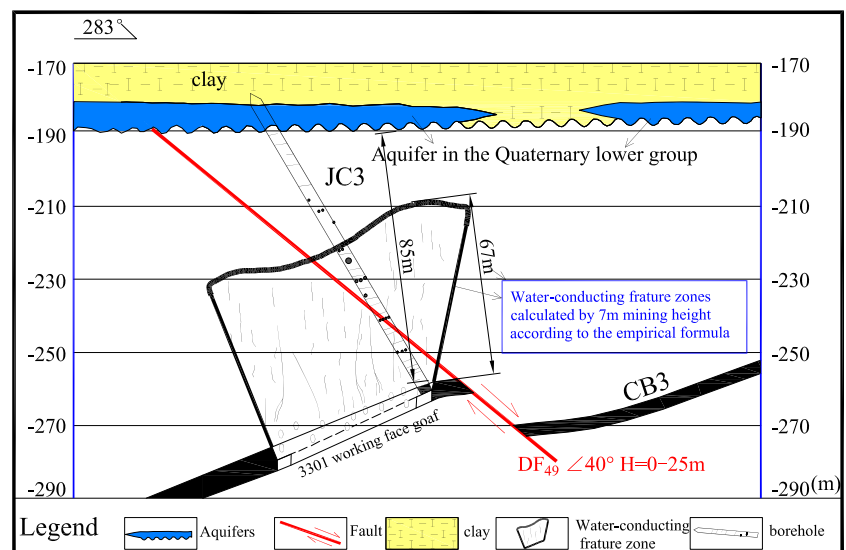
Methodology

Due to the limitations of the empirical formula application, the FLAC3D numerical simulation software was applied to study the mechanism of fault activation. FLAC3D can intuitively reflect the stress distribution of the roof in coal seam mining, and can well reveal the failure process of the roof and the disturbance to the fault when mining near the fault (Xu et al. 2015), which is of great guiding significance for the rational retention of the coal pillar. FLAC3D numerical simulation not only helps to study the mechanism of water inrush accident that has already occurred but also helps to guide the safe mining in future working faces, to predict the height of water-conducting fracture zones and has also achieved satisfactory results. The input data included the stratum and rock formation from the exploration boreholes, the data and characteristic of DF₄₉ fault from mining exposure and three-dimensional seismic exploration, and the mechanical properties. The data were extracted from the exploration reports at different stages, which are provided by the Department of Geology and Survey in Xinhe CM.

3D model establishment

In the process of numerical simulation, it is impossible to fully reflect the actual situation due to the influence of geological

Fig. 7 Sketch of position between fault and water-conducting fracture zone



structure and formation composition. Reasonable simplification of the actual situation is required to meet the needs of our research and to make the numerical simulation results reflect the actual situation as much as possible. This numerical simulation is based on the following assumptions:

- 1) The strata with similar lithology and mechanical parameters are classified into a group without considering the influence between adjacent strata.
- 2) The upper part of the model is applied vertical load instead of overburden weight.

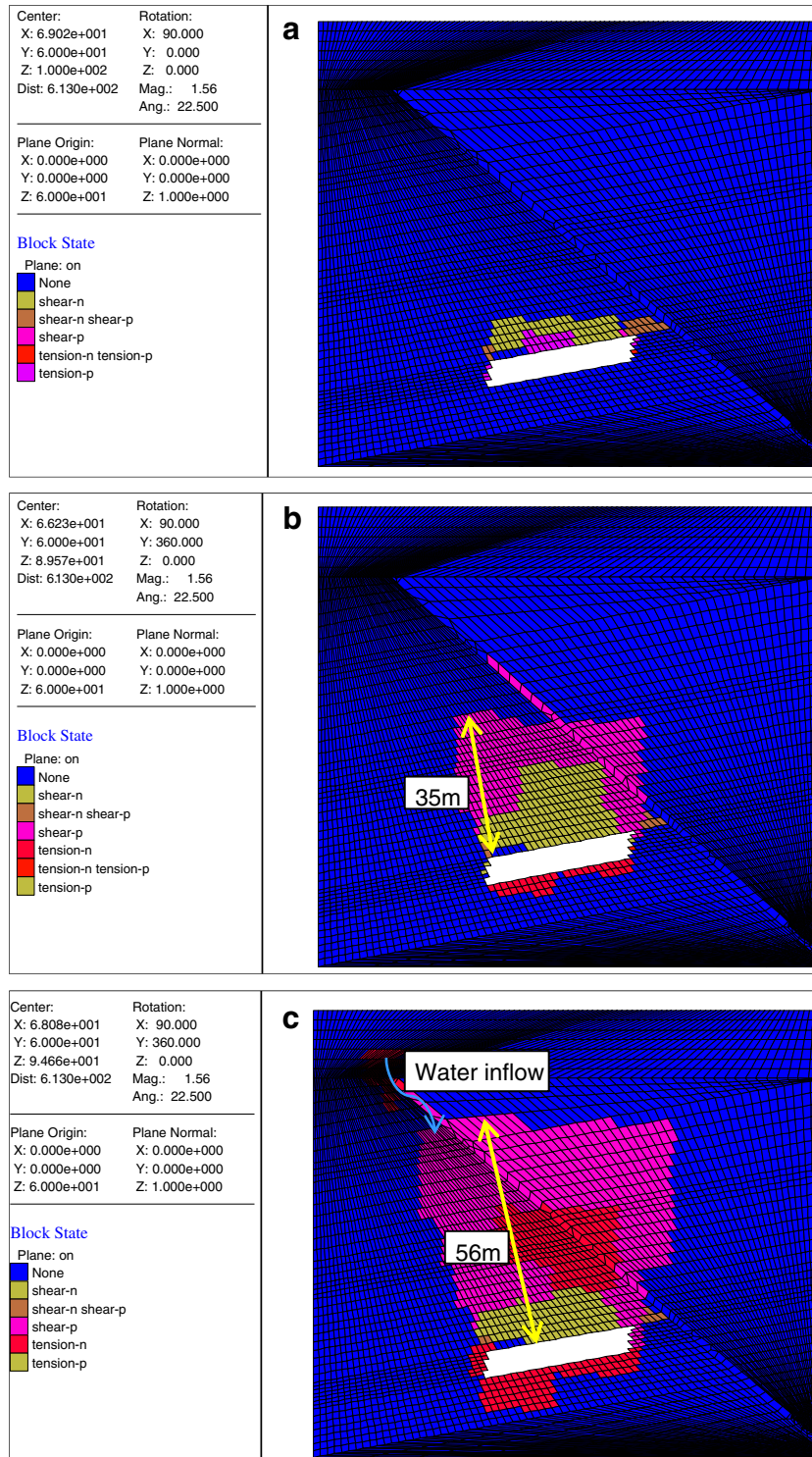


Fig. 8 Plastic failure zone diagram with mining 10 m (A), 20 m (B) and 35 m (C)

First, a mechanical conceptual excavation model is established according to the coal seam mining process. Horizontal movement is limited on the side of the model, and vertical movement is limited on the bottom of the model. Vertical load is applied on the upper part of the model to simulate the weight of overburden rock as required. For normal rock mass, the stress before coal seam mining is in a relatively equilibrium state. The model must first reach a balance state of initial force before the model changes, set initial conditions and boundary conditions, carry out initial balance calculation, and judge whether the model is balanced by the convergence state of the maximum unbalanced force approaching zero.

The model established in this simulation is based on the actual structure and stratigraphy exposed to the section of the 3301 working face. The 3301 working face is closer to but under fault DF₄₉ (300°∠40°, drop height is 0 to 25 m), belonging to near-fault coal seam mining. Based on the conceptual model, a fault-under-plate mining model with a length of 200 m and a width of 138 m and a model height of 120 m was established. The three-dimensional model is divided into 568,080 three-dimensional units, with a total of 587,736 nodes (please see electronic supplementary material, Fig. 10 and Table 1). What needs to be particularly stated is that the model is calibrated and the parameters resulted from the calibrations.

Simulation results and analysis

The no. 3301 working face is arranged substantially along the strike of the DF₄₉ fault, the model profile is perpendicular to the fault and the working face, and the working face with width 32 m, and length 100 m is set, according to the actual mining situation to carry out simulated mining, pre-mining at 31 m, encountering water problems, leaving 23-m pillars, and continuing mining 34 m. The stress maps and plastic area maps selected in the analysis below are cross-sectional views of the middle of the working face mining area perpendicular to the working face strike.

The plastic failure zone diagram with mining at 10 m (A), 20 m (B), and 35 m (C) are shown in Fig. 8. A stress arch appeared around the working face; there are stress concentration areas on both sides of the working face, and the stress of the fault increases especially where the fault roof is in contact with the Quaternary formation. Figure 8 (A) shows that the plastic failure occurs in the range of 3 to 7 m on top of the working face, and the failure zone is close to the fault, but the fault has not yet been plasticized; Fig. 8 (B) shows that the destruction of roof and floor intensifies and the scope of roof damage expands. The maximum height of the plastic failure zone is 35 m, and the plastic failure zone appears on the fault plane. In particular, there is a separate plastic failure zone above the plastic failure zone on the roof, indicating that the fault has a partial activation phenomenon. The height of the

plastic damage zone increased to 56 m, as shown in Fig. 8 (C), and the area of the plastic fracture zone of the fault plane is expanded, and the plastic destruction zone appears in the upper part of the fault to the bottom of the Quaternary, which indicates that the upper part of the fault is activated and the local failure zone is connected with the lower aquifers in Quaternary; therefore, the water inrush pathway formed (Zhang et al. 2018b), and large amounts of mine water were released from the calcareous cementation aquifer in Quaternary. Therefore, the mine water inrush source and pathway in the accident were identified which contribute to make fine countermeasures such as grouting the water inrush pathway.

Conclusions

This paper presents a case study identifying the source and pathway for a mine water inrush that occurred at the 3301 working face at Xinhe CM in Shandong province, China. The chronological water inrush process was described. In-depth analysis was performed of the characteristics of water flow rates, dynamic monitoring data of water levels in different aquifers, geochemical testing results, and observations in exploration boreholes. The multiple lines of evidence suggest that the source of water inrush originated from the Lower Quaternary porous aquifer. Solution cavities were observed to have increased the permeability and porosity in this aquifer. Karstification contributed greatly to the amount of water available in this source aquifer.

The movement law of roof strata in coal seam mining and the development height of water-conducting fracture zones in the roof were studied in detail. Based on the empirical equation recommended in the “Guidelines,” the water-conducting fracture zones would not reach the Quaternary aquifer under conditions without faults. However, the existence of a low-angle fault, DF₄₉, resulted in an increase in the height of the water-conducting fracture zones because of reactivation of the fault.

The empirical equation for calculating the mining-induced fractured height is no longer valid where faults are present in a working face. Instead, the numerical modeling as proposed in this paper should be used. In this paper, the mechanism of fault reactivation was studied with numerical simulation by FLAC3D in response to low-angle fault footwall mining. When the upper deck is under a normal fault, CB3 mining caused the mining-induced fracture zone to extend to the fault location, which leads to the change of the fault stress state, the fault plane, and the surrounding fissure expansion and connectivity. On the other hand, a prolific aquifer is present in the Lower Quaternary formation at the top of the fault. The seepage is concentrated in the fault plane under the water–rock interaction. When the top seepage area, the fault plane, and the fractured zone are hydraulically connected, water in the

Lower Quaternary aquifer flows along the fault and the mining-induced fractures into the mining space, causing water inrush accident. This study can provide reference for other water inrush accidents in Xinhe CM and has important practical significance for preventing water inrush in the coal mine. The lessons learned from this case will provide reference for engineers who deal with similar groundwater inrush issues in deep underground coal mines. In addition, the results facilitate better environmental decision-making on grouting the water inrush pathway and insulating the water inrush resource.

Acknowledgements The authors would like to thank technicians in the Department of Geology and Survey in Xinhe Coal Mine. We thank anonymous reviewers for detailed comments on the draft, all thorough reviews that greatly benefited the manuscript.

Funding information This research was financially supported by the National Key R&D Program of China (No. 2017YFC0804101), National Natural Science Foundation of China (Nos. 41402250 and 41702305), Graduate Science and Technology Innovation Project of Shandong University of Science and Technology (No. SDKDYC180319), and Taishan Scholar Talent Team Support Plan for Advantaged & Unique Discipline Areas.

References

- Bu WK (2009) Research on mechanical mechanism of fault activation and water inrush from faults in mining floor. Doctoral thesis. China University of Mining and Technology (in Chinese with English abstract)
- Bukowski P (2011) Water hazard assessment in active shafts in Upper Silesian coal basin mines. *Mine Water Environ* 30(4):302–311. <https://doi.org/10.1007/s10230-011-0148-2>
- Cetin M (2016) Sustainability of urban coastal area management: a case study on Cide. *J Sustain Forest* 35(7):527–541. <https://doi.org/10.1080/10549811.2016.1228072>
- Cetin M, Adiguzel F, Kaya O, Sahap A (2018) Mapping of bioclimatic comfort for potential planning using GIS in Aydin. *Environ Dev Sustain* 20(1):361–375. <https://doi.org/10.1007/s10668-016-9885-5>
- Chen T, Clauser C, Marquart G, Willbrand K, Hiller T (2018) Upscaling permeability for three-dimensional fractured porous rocks with the multiple boundary method. *Hydrogeol J* 26:1903–1916. <https://doi.org/10.1007/s10040-018-1744-z>
- Cheng JL, Sun XY, Gong Z, Gao F, Kong XR (2013) Numerical simulations of water-inrush induced by fault activation during deep coal mining based on fluid–solid coupling interaction. *Disaster Adv* 6: 10–14
- Guo QG (2016) Research on China's coalmine safety regulatory capture: formation mechanism, double impact and governance effect. Ph. D Thesis, Dongbei University of Finance and Economics (in Chinese with English abstract)
- Guo WJ, Zhao JH, Yin LM, Kong DZ (2017) Simulating research on pressure distribution of floor pore water based on fluid-solid coupling. *Arab J Geosci* 10(1):5–18. <https://doi.org/10.1007/s12517-016-2770-6>
- Huang PH, Chen JS (2011) Fisher identify and mixing model based on multivariate statistical analysis of mine water inrush sources. *J China Coal Soc* 36:131–136 (in Chinese with English abstract)
- Huang N, Jiang YJ, Liu RC, Li B (2017a) Estimation of permeability of 3-d discrete fracture networks: an alternative possibility based on trace map analysis. *Eng Geol* 226:12–19. <https://doi.org/10.1016/j.engeo.2017.05.005>
- Huang PH, Wang XY, Han SM (2017b) Recognition model of ground-water inrush source of coal mine: a case study on Jiaozuo coal mine in China. *Arab J Geosci* 10:323. <https://doi.org/10.1007/s12517-017-3099-5>
- Jiang LS, Sainoki A, Mitri H, Ma NJ, Liu HT, Hao Z (2016) Influence of fracture-induced weakening on coal mine gateroad stability. *Int J Rock Mech Min Sci* 88:307–317. <https://doi.org/10.1016/j.ijrmmms.2016.04.017>
- Jin DW, Liu YF, Liu ZB, Cheng JY (2013) New progress of study on major water inrush disaster prevention and control technology in coal mine. *Coal Sci Technol* 41:25–29 (in Chinese with English abstract)
- Kaya E, Agca M, Adiguzel F, Cetin M (2018) Spatial data analysis with R programming for environment. *Hum Ecol Risk Assess*. <https://doi.org/10.1080/10807039.2018.1470896>
- Krzysztof P, Kazimierz R, Piotr C (2016) Causes and effects of uncontrolled water inrush into a decommissioned mine shaft. *Mine Water Environ* 35:128–135. <https://doi.org/10.1007/s10230-015-0360-6>
- LaMoreaux JW, Wu Q, Zhou WF (2014) New development in theory and practice in mine water control in China. *Carbonates Evaporites* 29: 141–145. <https://doi.org/10.1007/s13146-014-0204-7>
- Lei GW, Yang CH, Wang GB, Chen SW, Wei X, Huo L (2016) The development law and mechanical causes of fault influenced zone. *Chin J Rock Mech Eng* 35:231–241 (in Chinese with English abstract)
- Li LC, Tang CA, Liang ZZ, Ma TH, Zhang YB (2009) Numerical analysis of pathway formation of groundwater inrush from faults in coal seam floor. *Chin J Rock Mech Eng* 28:290–297 (in Chinese with English abstract)
- Li T, Mei TT, Sun XH, Lv YG, Sheng JQ, Cai M (2013) A study on a water-inrush incident at Laohutai coalmine. *Int J Rock Mech Min Sci* 59:151–159. <https://doi.org/10.1016/j.ijrmmms.2012.12.002>
- Miao XX, Wang CS, Bai HB (2010) Hydrogeologic characteristics of mine water hazards in Shendong mining area. *J Min Safety Eng* 27:285–291 +298 (in Chinese with English abstract)
- Qi YM, Li MZ, Li KJ, Yeh T-CJ (2017) Spatiotemporal development of mine water inrush and its mechanism—a case study in Ganhe coal mine, Shanxi, China. *Arab J Geosci* 10:433. <https://doi.org/10.1007/s12517-017-3216-5>
- Qiao W, Li WP, Li T, Chang JY, Wang QQ (2017) Effects of coal mining on shallow water resources in semiarid regions: a case study in the Shennan mining area, Shaanxi, China. *Mine Water Environ* 36(1): 104–113. <https://doi.org/10.1007/s10230-016-0414-4>
- Rapantova N, Swiatoslaw K, Arnost G, Christian W (2012) Quantitative assessment of mine water sources based on the general mixing equation and multivariate statistics. *Mine Water Environ* 31:252–265. <https://doi.org/10.1007/s10230-012-0192-6>
- State Coal Industry Bureau (2017) Guideline for coal pillar retention and pressure coal mining in buildings, water bodies, railways and major roadways. China Coal Industry Press, Beijing (in Chinese with English abstract)
- Sui WH, Liu JY, Yang SG, Chen ZS, Hu YS (2011) Hydrogeological analysis and salvage of a deep coalmine after a groundwater inrush. *Environ Earth Sci* 62:735–749. <https://doi.org/10.1007/s12665-010-0562-y>
- Sun WJ, Wu Q, Liu HL, Jiao J (2015) Prediction and assessment of the disturbances of the coal mining in Kailuan to karst groundwater system. *Phys Chem Earth* 89–90:136–144. <https://doi.org/10.1016/j.pce.2015.10.008>
- Sun WJ, Zhou WF, Jiao J (2016) Hydrogeological classification and water inrush accidents in China's coal mines. *Mine Water Environ* 35:214–220. <https://doi.org/10.1007/s10230-015-0363-3>
- Sun WB, Zhang SC, Guo WJ, Liu WT (2017) Physical simulation of high-pressure water inrush through the floor of a deep mine. *Mine*

- Water Environ 36:542–549. <https://doi.org/10.1007/s10230-017-0443-7>
- Surinaidu L, Rao VVSG, Ramesh G (2013) Assessment of groundwater inflows into Kuteswar limestone mines through flow modeling study, Madhya Pradesh, India. *Arab J Geosci* 6:1153–1161. <https://doi.org/10.1007/s12517-011-0421-5>
- Tan YL, Ning JG, Li HT (2012) In situ explorations on zonal disintegration of roof strata in deep coalmines. *Int J Rock Mech Min Sci* 49(1): 113–124. <https://doi.org/10.1016/j.ijrmmms.2011.11.015>
- Wang G, Wu MM, Wang R, Xu H, Song X (2017) Height of the mining-induced fractured zone above a coal face. *Eng Geol* 216:140–152. <https://doi.org/10.1016/j.enggeo.2016.11.024>
- Wei JC, Xiao LL, Niu C, Yin HY, Shi LQ, Han J, Duan FT (2015) Characteristics analysis of the correlation factors of China mine water hazard accidents in 2001–2013. *China Sciencepaper* 10:336–341 (in Chinese with English abstract)
- Wei JC, Wu FZ, Yin HY, Guo JB, Xie DL, Xiao LL, Zhi HF, Liliana L (2017) Formation and height of the interconnected fractures zone after extraction of thick coal seams with weak overburden in western China. *Mine Water Environ* 36(1):59–66. <https://doi.org/10.1007/s10230-016-0396-2>
- Wu Q, Xu H, Pang W (2008) GIS and ANN coupling model: an innovative approach to evaluate vulnerability of karst water inrush in coalmines of North China. *Environ Geol* 54:937–943. <https://doi.org/10.1007/s00254-007-0887-3>
- Wu Q, Fan SK, Zhou WF, Liu SQ (2013) Application of the analytic hierarchy process to assessment of water inrush: a case study for the No. 17 coal seam in the Sanhejian Coal Mine, China. *Mine Water Environ* 32:229–238. <https://doi.org/10.1007/s10230-013-0228-6>
- Wu Q, Guo XM, Shen JJ, Xu S, Liu SQ, Zeng YF (2017a) Risk assessment of water inrush from aquifers underlying the Gushuyuan coal mine, China. *Mine Water Environ* 36:96–103. <https://doi.org/10.1007/s10230-016-0410-8>
- Wu Q, Mu WP, Xing Y, Qian C, Shen JJ, Wang Y, Zhao DK (2017b) Source discrimination of mine water inrush using multiple methods: a case study from the Beiyangzhuang Mine, Northern China *B Eng Geol Environ*. <https://doi.org/10.1007/s10064-017-1194-1>
- Xu ZM, Sun YJ, Gong SY, Zhu ZK (2012) Monitoring and numerical simulation of formation of water inrush pathway caused by coal mining above confined water with high pressure. *Chin J Rock Mech Eng* 31:1698–1704 (in Chinese with English abstract)
- Xu XH, Lv JG, Liu C, Bai RC, Li S (2015) Influence law of fault activation induced by coal extraction based on characteristics parameters of thrust fault. *J Chongqing Univ* 38:107–115 (in Chinese with English abstract)
- Xu ZM, Sun YJ, Gao S, Zhao XM, Duan RQ, Yao MH, Liu Q (2018) Groundwater source discrimination and proportion determination of mine inflow using ion analyses: a case study from the Longmen Coal Mine, Henan Province, China. *Mine Water Environ* 37:385–392. <https://doi.org/10.1007/s10230-018-0512-6>
- Yang B, Sui W, Duan L (2017) Risk assessment of water inrush in an underground coal mine based on GIS and fuzzy set theory. *Mine Water Environ* 36:617–627. <https://doi.org/10.1007/s10230-017-0457-1>
- Yin HY, Wei JC, Lefticariu L, Guo JB, Xie DL, Li ZL, Zhao P (2016) Numerical simulation of water flow from the coal seam floor in a deep longwall mine in China. *Mine Water Environ* 35:243–252. <https://doi.org/10.1007/s10230-016-0385-5>
- Yin HY, Zhou WF, LaMoreaux JW (2018a) Water inrush conceptual site models for coal mines of China. *Environ Earth Sci* 77:746. <https://doi.org/10.1007/s12665-018-7920-6>
- Yin HY, Shi YL, Niu HG, Xie DL, Wei JC, Lefticariu L, Xu SX (2018b) A GIS-based model of potential groundwater yield zonation for a sandstone aquifer in the Juye Coalfield, Shangdong, China. *J Hydrol* 557:434–447. <https://doi.org/10.1016/j.jhydrol.2017.12.043>
- Yu B, Zhao J, Xiao HT (2017) Case study on overburden fracturing during longwall top coal caving using microseismic monitoring. *Rock Mech Rock Eng* 50(2):1–5. <https://doi.org/10.1007/s00603-016-1096-8>
- Zhang JC (2005) Investigations of water inrushes from aquifers under coal seams. *Int J Rock Mech Min Sci* 42:350–360. <https://doi.org/10.1016/j.ijrmmms.2004.11.010>
- Zhang HR, Zhou RF, Guo DZ, Du PJ (2005) Investigation on predicting roof water gush in coal mines based on multi-factor analysis. *J China Univ Min Technol* 34:112–116 (in Chinese with English abstract)
- Zhang WQ, Li B, Yuan JD (2016) Detection and evaluation of crack development near the fault zone under the influence of coal mining. *Electron J Geotech Eng* 21(22):6841–6850
- Zhang SC, Guo WJ, Li YY, Sun WB, Yin DW (2017a) Experimental simulation of fault water inrush channel evolution in a coal mine floor. *Mine Water Environ* 36:443–451. <https://doi.org/10.1007/s10230-017-0433-9>
- Zhang WQ, Li B, Zhang GB, Li ZL (2017b) Investigation of water-flow fracture zone height in fully mechanized cave mining beneath thick alluvium. *Geotech Geol Eng* 35:1745–1753. <https://doi.org/10.1007/s10706-017-0205-0>
- Zhang SC, Guo WJ, Li Y (2017c) Experimental simulation of water-inrush disaster from the floor of mine and its mechanism investigation. *Arab J Geosci* 10(22):503–513
- Zhang WJ, Li SC, Wei JC, Zhang QS, Liu RT, Zhang X, Yin HY (2018a) Grouting rock fractures with cement and sodium silicate grout. *Carbonates Evaporites* 33(2):211–222. <https://doi.org/10.1007/s13146-016-0332-3>
- Zhang DY, Sui WH, Liu JW (2018b) Overburden failure associated with mining coal seams in close proximity in ascending and descending sequences under a large water body. *Mine Water Environ* 37:322–335. <https://doi.org/10.1007/s10230-017-0502-0>
- Zhao TB, Yin YC, Tan YL (2012) Safe mining and new prediction model in coal seam with rock burst induced by roof. *Disaster Adv* 5(4): 961–965
- Zhou QL, Juan H, Arturo H (2017) The numerical analysis of fault-induced mine water inrush using the extended finite element method and fracture mechanics. *Mine Water Environ* 37:185–195. <https://doi.org/10.1007/s10230-017-0461-5>